Laser Doppler interferometer based on a solid Fabryâ€“Perot etalon for measurement of surface velocity in shock experiments

Arrigoni, M.; Monchalin, J. -P.; Blouin, A.; KrÃ¼ger, S. E.; Lord, M.

Publisher's version / Version de l'éditeur:
https://doi.org/10.1088/0957-0233/20/1/015302
Measurement Science & Technology, 20, 1, 2009

Laser Doppler interferometer based on a solid Fabry–Perot etalon for measurement of surface velocity in shock experiments

2009 Meas. Sci. Technol. 20 015302

(http://iopscience.iop.org/0957-0233/20/1/015302)

Meas. Sci. Technol. **20** (2009) 015302 (7pp) doi:10.1088/0957-0233/20/1/015302

Laser Doppler interferometer based on a solid Fabry–Perot etalon for measurement of surface velocity in shock experiments

M Arrigoni[1], J-P Monchalin, A Blouin, S E Kruger[2] and M Lord

Industrial Materials Institute, National Research Council of Canada, 75 de Mortagne blvd, Quebec, J4B 6Y4, Canada

E-mail: silvio.kruger@cnrc-nrc.gc.ca

Received 17 June 2008, in final form 6 October 2008
Published 8 December 2008
Online at stacks.iop.org/MST/20/015302

Abstract
This study presents an original optical system designed for measuring the free surface velocity for shock wave diagnostics. The system is based on a solid Fabry–Perot etalon interferometer coupled to a tunable, single frequency laser. The setup assembled for this purpose can measure velocities up to 200 m s^{-1} and has a resolution time of about 1 ns. This system was validated in shock experiments performed on thin aluminum samples. The shock waves were generated by a pulsed laser on a water confinement configuration and the surface velocity was measured on the opposite side of the sample. The signals obtained are in good agreement with numerical simulation and results found in the literature. This system presents an interesting alternative to the velocity interferometer system for any reflectors (VISAR) commonly used in shock experiments.

Keywords: Fabry–Perot interferometer, shock wave, optical velocimeter

(Some figures in this article are in colour only in the electronic version)

1. Introduction

The physics of shock waves propagating in a material is properly described by three thermodynamic variables (E, P, ρ), which are respectively the internal energy, the hydrodynamic pressure and the material density, and two kinetic variables (D, u), which are respectively the shock wave velocity and the material—or particle—velocity [1].

Several methods have been used for the measurement of the free surface velocity. A successful and reliable method has been an optical interferometric technique based on the Doppler effect. The technique uses the laser Doppler interferometer (LDI) and allows the measurement of material velocity according to the Doppler effect. When the shock material motion breaks out at the surface illuminated by a laser beam, the reflected or scattered laser light is frequency shifted by the Doppler effect from an incident frequency ν_0 to frequency ν as follows:

$$\frac{\nu - \nu_0}{\nu_0} = \frac{2(u - u_0)}{c}, \tag{1}$$

where u is the instantaneous material velocity to be measured, u_0 is the initial material velocity and c the speed of light.

LDIs are very useful diagnostic tools for a variety of industrial applications. Being laser based, they operate at a distance and allow testing to be easily automated. Several kinds of LDI have been developed for shock or ultrasonic measurements and have been described in several review papers [2–4]. Michelson interferometers in which the probed surface acts as a mirror of the interferometer, either homodyne or heterodyne, were found to present several difficulties. In the homodyne configuration, they were found too sensitive to environmental vibrations. The heterodyne configuration, on the other hand, makes the measurement of high material velocities hard because of the difficulty in counting the large number of fringes involved in this case.

[1] Current address: ENSIETA LBMS, 2 rue François Verny, 29806 Brest Cedex 9, France.
[2] Author to whom any correspondence should be addressed.

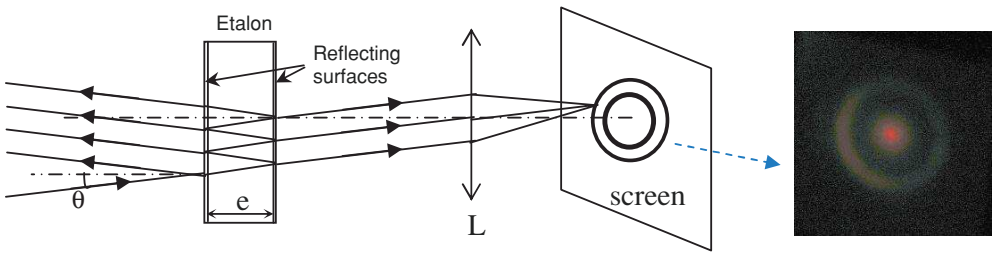

Figure 1. Principle of the Fabry–Perot interferometer as used in optical spectroscopy. A series of rings can be observed in the focal plane of the lens if the source gives a sufficient angular range. The detector (not represented here) is located behind an aperture centered on the rings so as to receive only part of the central fringe.

Two-wave interferometers (Michelson or Mach–Zehnder) with different arm lengths working as light frequency analyzers were found very successful for shock measurements and to a lesser extent for ultrasound detection, due to the relatively low ultrasonic frequencies found in the usual non-destructive ultrasonic testing. In these interferometers the light collected from the probed surface is split into two beams which are given different delays by the different arm lengths and then made to interfere. By adding properly to the long arm a glass slab (or the like, in practice an optical etalon with antireflection coatings), the etendue or throughput (which is somehow the capacity to process effectively light from a diffuse source) can be increased, making very efficient devices. The most well-known interferometer of this type is the VISAR (velocity interferometer system for any reflectors) [5], which since its introduction has gone through several evolutions [6]: multipoint VISAR, line VISAR, fixed cavity VISAR, etc. It allows the measurement of material velocity with 1% accuracy and with a resolution better than 1 ns. By changing the etalon located in the long arm, it is then possible to increase the range of measurable velocities, from less than 100 m s^{-1} to more than 10 km s^{-1}.

Multiple-wave interferometers, i.e. Fabry–Perots, producing multiple delayed waves can be used as well. The confocal version, which provides enhanced etendue, and is used with rather long cavity lengths (typically 50 cm or 1 m) is now a standard device for detecting ultrasound in laser ultrasonics [7]. Planar Fabry–Perots have been used for shock wave measurements in conjunction with a streak camera which monitors the displacement of Fabry–Perot ring fringes in the focal plane of a lens versus time [5, 8]. They have also been developed for multi-point measurements and the results obtained were found in good agreement with those obtained with a VISAR.

In this paper, we report the use of a solid Fabry–Perot planar etalon for shock measurement without a streak camera. This system allows measuring particle velocities ranging from less than 0.3 m s^{-1} to 200 m s^{-1}. We also report results obtained with this detecting device on laser-induced shock experiments performed on 1 mm thick aluminum samples. These results are also compared with theoretical results obtained with a numerical code and other previously reported results.

2. Laser Doppler interferometer based on a solid Fabry–Perot etalon

2.1. Principle

The reported device is based on a solid Fabry–Perot planar etalon. The principle of operation is shown in figure 1. The device combines the conventional use of a Fabry–Perot in optical spectroscopy [9–11] with its use for detecting ultrasound. In spectroscopy, spectral information on the light source is obtained by selecting with a circular aperture, part of the central fringe pattern in the focal plane of a lens. The spectrum of the source is obtained by scanning the path difference (i.e. the Fabry–Perot optical thickness). Here, like in the detection of ultrasound, the frequency of the source is actually varied with time due to the Doppler effect produced by the surface motion and the Fabry–Perot has a fixed thickness. The signal related to the surface motion appears on the detector behind the aperture at the center of the fringe pattern.

When the light frequency ν is swept (or alternatively when the Fabry–Perot optical thickness is varied) resonance peaks are observed, as shown in figure 2. These peaks are separated by the free spectral range (FSR) of the etalon given by equation (2), where e is the thickness of the etalon, n its refractive index and c is the speed of light in the vacuum:

$$\mathrm{FSR} = \frac{c}{2ne}. \tag{2}$$

The free spectral range is the inverse of the time delay between interfering waves $\tau = 1/\mathrm{FSR}$. The full width at half maximum of the peaks, denoted w, is equal to the FSR divided by the Fabry–Perot finesse F, which depends upon the surface reflectivity and planarity of the etalon surfaces. By stabilizing the optical frequency at half maximum of a resonance peak of the etalon, a modulation of the optical frequency results in a modulation of the optical intensity transmitted through the Fabry–Perot. This optical intensity variation (ΔI) and the optical frequency variation ($\Delta\nu$) are linked by the slope of resonance peak (k) at half maximum:

$$\Delta I = k\Delta\nu \tag{3}$$

with $k = q\frac{I_0}{w}$,where I_0 is the incident intensity on the Fabry–Perot and q is a value that depends on the Fabry–Perot parameters and the optical setup. The calculated value of q is unity for an ideal lossless Fabry–Perot illuminated by a uniform plane wave at near normal incidence. For operation in practical conditions, reliable values of q, w and then k

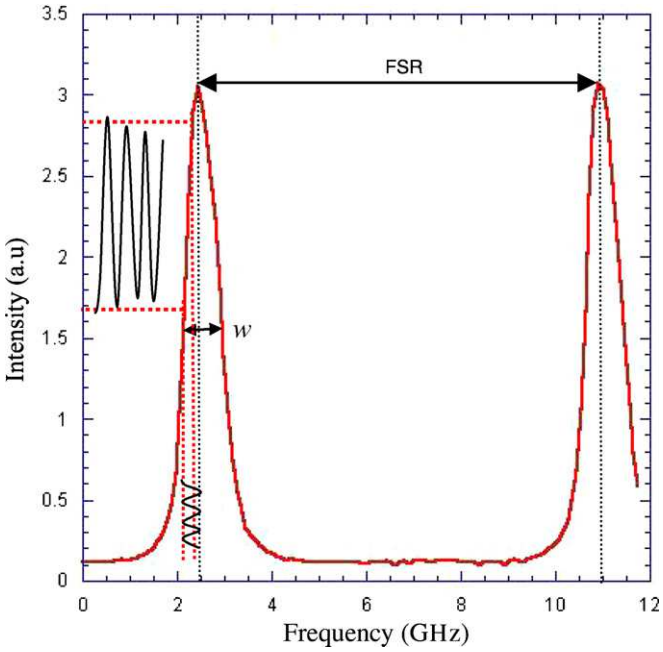

Figure 2. Resonance peaks of the Fabry–Perot etalon used. The optical frequency of the detection laser is tuned to half maximum of a resonance peak to provide demodulation.

are obtained by monitoring the Fabry–Perot transmission by scanning the laser frequency, giving trustworthy parameters for the actual optical measurement setup. Since, the variation of material velocity Δu is linked to the variation of optical frequency $\Delta\nu$ by the Doppler effect, as depicted in equation (1), the linear relationship between the optical intensity variation and the material velocity is given by:

$$\Delta u = \frac{\lambda}{2}\Delta v = \frac{\lambda}{2k}\Delta I. \tag{4}$$

As shown in equation (3), the slope k, which gives the calibration factor between the optical intensity variation and the material surface velocity depends on the optical intensity (I_0) incident on the Fabry–Perot. Since the optical reflectivity of the inspected material may vary from one location to the other, the intensity I_0 must be monitored to correct the value of k.

It should be noted that this simple relationship between the change of intensity and the surface velocity is not valid for velocity variations that occur on a time scale shorter than the response time of the interferometer, which can be evaluated as equal to $F\tau$. Alternatively, this means that the surface motion that is probed should encompass frequencies smaller than the peak width w. This is in agreement with the theory of detection of ultrasound with a Fabry–Perot, which shows that the signal is proportional to velocity (or varies linearly with frequency for a given displacement amplitude) when the ultrasonic frequency is lower than a peak width w. Linearity is also limited by the velocity (or Doppler shift) excursion. When the Doppler shift becomes close to about $w/2$, the change of intensity saturates and then becomes negative as could easily be guessed from figure 2. We use a solid etalon Fabry–Perot instead of one made of two parallel plates, which would have required a precise alignment system (usually made by three piezoelectric pushers) to make the two plates parallel. A solid etalon does not require any alignment and is also weakly dependent on room temperature variations. However, this requires that the detection laser source be frequency tunable.

2.2. Implementation

The optical layout of the detection setup with the Fabry–Perot etalon is shown in figure 3. The detection laser is a commercially available laser source developed for the industrial applications of laser ultrasonics. It comprises a monolithic single frequency Nd-YAG 500 mW seed laser which is amplified by double-pass flashlamp pumped Nd-YAG rod amplifiers to about 1 kW peak power. The output pulse duration is typically less than 100 μs, which is sufficient to properly capture the material free surface displacements produced by the shock wave. The seed laser is frequency tuned by thermal control of its Nd-YAG crystal. Such a slow thermal control is adequate since both the seed laser crystal and the Fabry–Perot etalon are very stable and drift very slowly in frequency. The beam at the output of the pulsed laser is sent into a 400 μm core optical fiber. The light exiting this fiber is projected onto the probed surface to a spot of about 400 μm in diameter. Scattered light is then collected and sent into a second 1 mm core diameter, 0.36 numerical aperture optical fiber. Light from this fiber then illuminates the etalon through the lens L1. A small fraction of the collected light is picked up in front of the etalon by a glass plate and is focused on a reference photodiode to compensate for surface reflectivity variations at different locations on the probed surface. This photodiode is also sufficiently fast to detect any changes of reflectivity that could occur during the shock wave arrival at the probed surface (e.g. a surface deformation that will change the light level collected as a function of time). Positive lens L3 and negative lens L4 make a combination with a long focal length, which results in ring fringes with a sufficiently large diameter for easy selection of part of the central fringe with a diaphragm of a few millimeters diameter. As shown in figure 3, light is then split unequally into two arms and sent to two photodetectors. One arm is for the measurements of the ultrasonic surface displacement and contains a fast photodiode with a bandwidth ranging from a few kHz to 800 MHz. The second arm is for the stabilization of the laser wavelength and is ended by a control photodetector, similar to the reference photodetector, to complete the stabilization feedback loop. Signals from all three photodiodes are digitized by an acquisition card at 2 GS s^{-1}.

We have used a 15.8 mm thick solid etalon having a FSR of about 8.5 GHz with high reflection coatings giving a finesse F of about 10.6 at $\lambda = 1.06$ μm. The peaks' width or bandwidth is then measured to be about 800 MHz. The delay time is then about 0.1 ns and response time about 1 ns. This system has therefore a resolution of about 1 ns and surface velocity variation on a time scale shorter than 1 ns cannot be adequately measured. According to the peak width and equation (3), the system is able to measure velocities up to 200 m s^{-1}, which is suitable for the experiments reported in the following section.

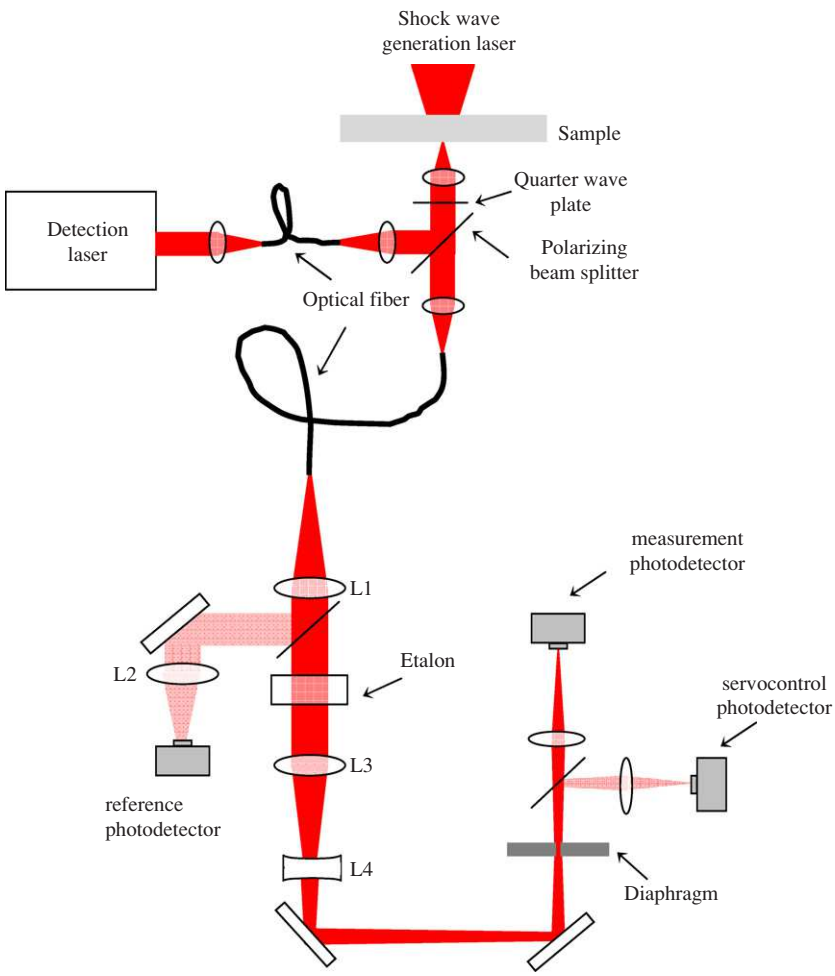

Figure 3. Optical layout of the detection setup.

3. Application to shocks generated in aluminum plates

3.1. Experimental setup

The experimental setup for shock wave generation and diagnostics is shown in figure 4. Shock wave generation is made with a Nd-YAG high energy pulsed laser which provides 10 ns at a half maximum Gaussian pulse of 2.4 J at an optical wavelength of $\lambda = 1.06\ \mu$m. It is commercially available table-top equipment that works at a repetition rate of 10 pulses per second. Laser shots are performed under a water confinement regime. This water confinement allows increasing both the shock pressure and duration [12]. The laser beam is focused on the sample surface, through a convergent lens, to a spot of about 2 mm in diameter. Energy losses due to the light absorption in the 3 mm thick water layer [13] and spurious reflection on optical components are about 0.5 J. In such conditions, Berthe [14] and Sollier [15] showed that the shock pressure could reach up to 5 GPa at a power density of 9 GW cm^{-2}. They also showed that the maximal power density that can be sent to a sample in the water confinement regime is about 9 GW cm^{-2}. For higher laser power densities, a breakdown phenomenon ionizes water and thus blocks the deposition of more laser energy.

Shock diagnostic from the surface velocity of the sample surface opposite to laser shock generation is performed as described in section 2. Generation and detection lasers are synchronized by a clock control unit. Because of the water confinement regime and the water splash on the front optics produced by the irradiation, the laser is operated in a single shot mode and the front optics is wiped after each shot. Signal acquisition is trigged by an avalanche photodiode picking up some light from the generation laser.

3.2. Results

Shots were performed on 1.07 mm thick Al AA5754 plates in the water confinement regime at various power densities ranging from 0.70 to 4.16 GW cm^{-2}. The impacted area was of 2 mm diameter and the velocity of the sample free surface with respect to the impacted area was measured with the Fabry–Perot etalon interferometer. Results are plotted on figure 5 where the measured surface velocity versus time is displayed.

For a given power density, at least three measurements were performed. The laser power density varies about 5% from shot to shot, which results in slight fluctuations of the measured velocity. Measurement fluctuations can then be estimated and then can be taken into account for numerical simulation.

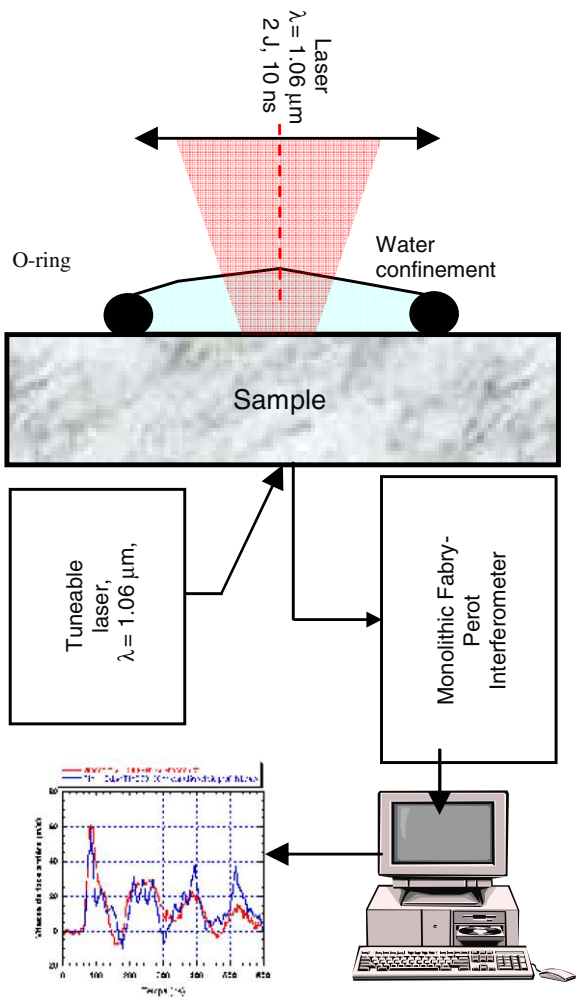

Figure 4. Experimental setup for the shock wave experiment.

The measurements of the Fabry–Perot etalon interferometer (figure 5) show the main features of shock wave propagation in a 1 mm Al sample. First, the signal amplitude increases with the incident power density, as expected. Second, peaks of two different origins can be extracted from the signals.

The highest peaks are regularly spaced by 330 ns, which is the reverberation time of the longitudinal wave through the sample 1.07 mm thickness. The average longitudinal wave velocity hence deduced is about $D = 6450$ m s^{-1}, which matches rather well the longitudinal velocity in aluminum.

Peaks of other origins are located between longitudinal peaks and are the occurrence of lateral waves evolving in the shock slipstream [16]. This situation occurs when the one-dimensional approximation no longer holds, that is when the diameter of the impacted area is smaller than two to three times the sample thickness. These lateral effects appear anyway after several reflections back and forth in the sample and they coincide with shear wave peaks, which are much lower in intensity.

Figure 5(*b*) shows a step in the slope of the first peak. This step is the breakout of the longitudinal elastic wave that is faster than the plastic wave and is known as the Hugoniot elastic limit, noted σ_{HEL}. This effect is due to the initial compression wave which induces, above the elastic limit, a plastic strain that propagates at a slower velocity than the elastic strain. The Hugoniot elastic limit has extensively been studied. The most common value is $\sigma_{\mathrm{HEL}} = 550$ MPa for aluminum [17], but strongly depends on the strain rate and the aluminum grade. For example, for Al 2024, the Hugoniot elastic limit is about 120 MPa [18] while it is 390 MPa [19] for the Al 7010 T6 grade, determined by bar impacts for various impact velocities. It has not been measured for aluminum AA 5754, but can be estimated from free surface velocity measurement by equation (5),

$$\sigma_{\mathrm{HEL}} = \frac{\rho_0 C_L u_{\mathrm{fs}}^{\mathrm{HEL}}}{2}, \tag{5}$$

where $u_{\mathrm{fs}}^{\mathrm{HEL}}$ is the free surface velocity at the step in the slope, C_L is the longitudinal sound velocity and ρ_0 is the initial density of the material (2685 kg cm^{-3} for aluminum AA 5754).

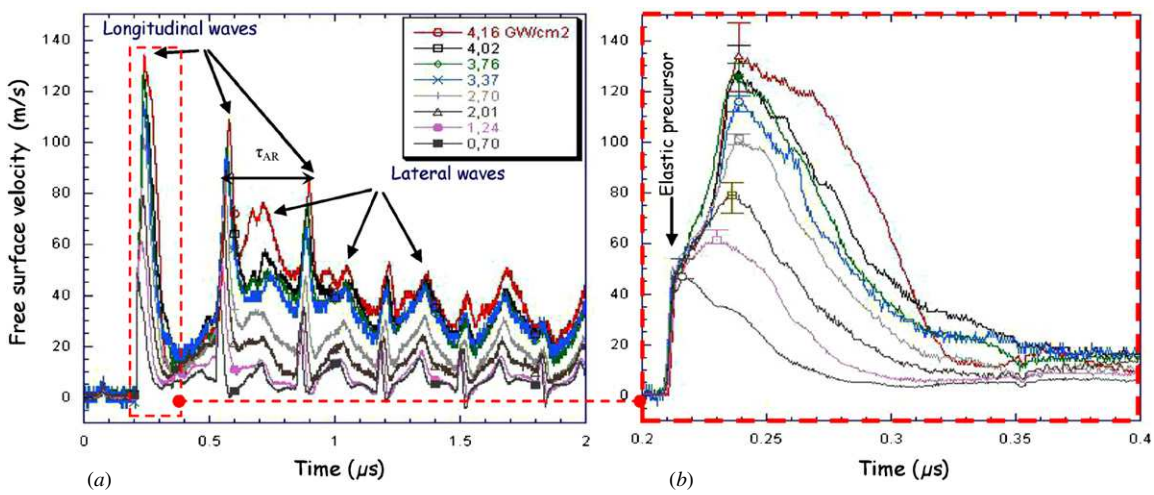

Figure 5. (*a*) Free surface velocity of Al AA5754 sample irradiated at various power densities in the water confinement regime, (*b*) enlargement of (*a*).

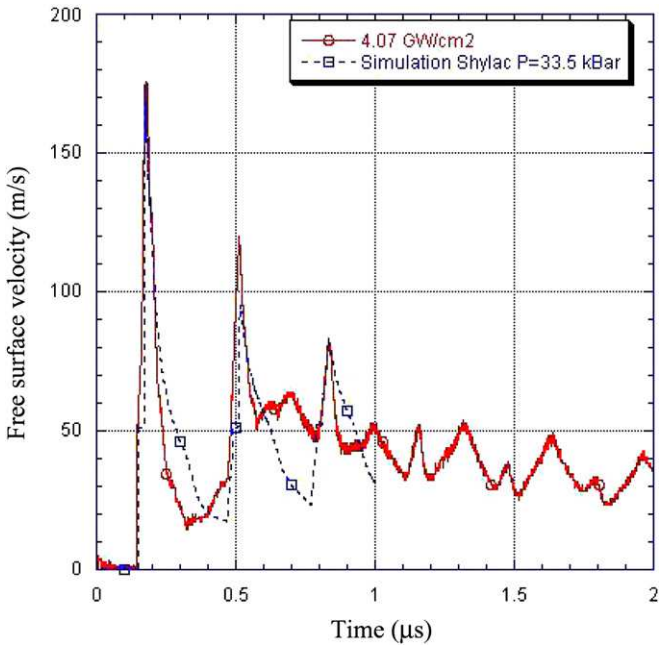

Figure 6. Comparison between experimental free surface velocity, at 4.07 GW cm^{-2} in the water confined regime on Al 1070 μm (continuous line), and free surface velocity computed with SHYLAC (dashed line).

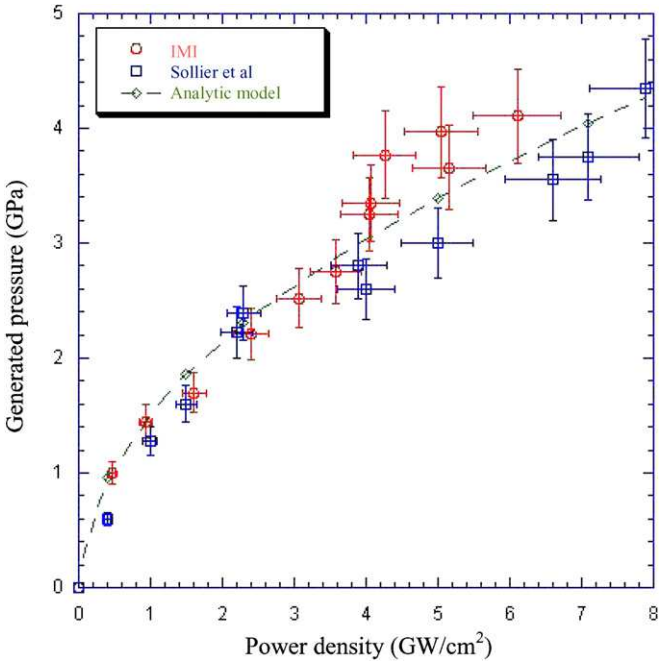

Figure 7. Comparison of experimental results from the present study (circles) with those obtained by Sollier [20] (squares) and its analytical model (dashed line).

In figure 5, the step representing the Hugoniot elastic limit is not a blatant horizontal step, so $u_{\mathrm{fs}}^{\mathrm{HEL}}$ is estimated between 53 and 66 m s^{-1}. The calculated Hugoniot elastic limit for aluminum AA 5754 from equation (5) is then between 446 and 555 MPa, which is in agreement with the literature.

Simulations were performed using the hydrodynamic Lagrangian code *SHYLAC* [20]. For each laser shot, the input parameter representing the energy deposited on the sample was chosen to match the computed surface velocities with experimental surface velocities. An example is shown in figure 6 for a laser power density of 4.07 GW cm^{-2}. The maximal incident pressure generated in the water confinement regime was then deduced. The calculated Hugoniot elastic limit was 491 MPa, in agreement with that deduced from experiments. From this set of experiments, a pressure versus power density curve was obtained and compared with the analytical model and previous experiments of Berthe [19] and Sollier [20] (figure 7):

$$P\,(\mathrm{GPa}) = 0.01\sqrt{\frac{\alpha}{\alpha+3}}\sqrt{Z\,(\mathrm{g\ cm^{-2}\,s^{-1}})}\sqrt{I_0\,(\mathrm{GW\,cm^{-2}})}, \tag{6}$$

where α is a coefficient of laser–matter interaction in the water confinement regime, which is close to 0.25 at wavelength $\lambda = 1.06\ \mu$m, Z is the acoustic impedance: $\frac{2}{Z} = \frac{1}{Z_{\mathrm{water}}} + \frac{1}{Z_{\mathrm{target}}}$ where $Z_i = \rho_{0i} \cdot C_{0i}$ is the acoustic impedance of the medium i at the initial state. ρ_{0i} and C_{0i} are respectively the density and the bulk sound velocity in the medium i at the initial state. The bulk velocity C_0 is calculated with the longitudinal C_L and transverse C_T velocities of sound, using relation (7),

$$\mathrm{C}_0 = \sqrt{C_L^2 - \tfrac{4}{3}C_T^2} \tag{7}$$

and I_0 is the incident power density.

The coefficient of laser–matter interaction α was estimated with SHYLAC and found closer to 0.25 for power densities above 4 GW cm^{-2} and closer to 0.22 below 4 GW cm^{-2}. These values are in agreement with Berthe [19] and Sollier's [20] values of around 0.25.

4. Conclusion

In this study we have presented an alternative laser Doppler interferometer to the widely used VISAR, for measuring the surface velocity of a material under shock. It is based on a Fabry–Perot etalon, which is monolithic, compact and affordable. The signal provided by the interferometer is directly proportional to the effective free surface velocity, which makes it easy to use.

Experiments were carried out in water confinement configuration on aluminum samples. Despite the fact that velocity signals have not been compared to those measured with a VISAR, the inverse approach shows that they are coherent in amplitude with the approach of Berthe [19]. They show main features that are usually observed in VISAR experiments: back and forth of longitudinal and lateral waves, Hugoniot elastic precursor. On this occasion we could also estimate the Hugoniot elastic limit of aluminum AA 5754 at around 500 MPa ± 50 MPa, which was corroborated by the numeric code SHYLAC.

Acknowledgment

The authors would like to thank L Berthe (LALP) and M Boustie (LCD) from CNRS for the useful information and advice they kindly provided.

References

[1] Zel'Dovich Ya B and Raizer Yu P 2002 *Physics of Shock Waves and High-Temperature Hydrodynamic Phenomena* (Mineola, NY: Dover)

[2] McMillan C F, Goosman D R, Parker N L, Steinmetz L L, Chau H H, Huen T, Whipkey R K and Perry S J 1988 Velocimetry of fast surfaces using Fabry–Perot interferometry *Rev. Sci. Instrum.* **59** 1–21

[3] Monchalin J-P 1986 Optical detection of ultrasound *IEEE Trans. Ultrason. Ferroelec. Freq. Control* **33** 485–99

[4] Dewhurst R J and Shan Q 1999 Optical remote measurement of ultrasound *Meas. Sci. Technol.* **10** 139–68

[5] Barker L M and Hollenbach R E 1972 Laser interferometry for measuring high velocities for any reflecting surface *J. Appl. Phys.* **43** 4669–75

[6] Barker L M 2000 The development of the VISAR and its use in shock compression science *AIP Conf. Proc.* **505** 11–7

[7] Monchalin J-P, Héon R, Bouchard P and Padioleau C 1989 Broadband optical detection of ultrasound by optical sideband stripping with a confocal Fabry–Perot *Appl. Phys. Lett.* **55** 1612–4

[8] Le Hiboux O 1998 Conception de chaînes vélocimétriques doppler multipoints miniaturisées. Application à la détonique *PhD Thesis* Conservatoire National des Arts et Métiers (in French)

[9] Scruby C B and Drain L E 1990 *Laser Ultrasonics, Techniques and Applications* (Bristol: Hilger)

[10] Hernandez G 1988 *Fabry–Perot Interferometers* (Cambridge: Cambridge University Press)

[11] Vaughan J M 1989 *The Fabry–Pérot Interferometer, History, Theory, Practice and Applications* (Bristol: Hilger)

[12] Fabbro R, Fournier J, Ballard P, Devaux D and Virmont J 1990 Physical study of laser-produced plasma in confined geometry *J. Appl. Phys.* **68** 775–81

[13] Kanayama K, Baba H, Endoh N and Nemoto T 1997 Spectral transmittance of water and sodium chloride water solution as working substance for a solar pond *Heat Transfer—Japan. Res.* **26** 1–15

[14] Berthe L, Fabbro R, Peyre P, Tollier L and Bartnicki E 1997 Shock waves from a water-confined laser-generated plasma *J. Appl. Phys.* **82** 2826–32

[15] Sollier A, Berthe L and Fabbro R 2001 Numerical modeling of the transmission of breakdown plasma generated in water during laser shock processing *Eur. Phys. J. AP* **16** 131–9

[16] Boustie M, Cuq-Lelandais J P, Bolis C, Berthe L, Barradas S, Arrigoni M, de Resseguier T and Jeandin M 2007 Study of damage phenomena induced by edge effects into materials under laser driven shocks *J. Phys. D: Appl. Phys.* **40** 7103–8

[17] Mc Queen R G, Marsh S P, Taylor J W, Fritz J N and Carter W J 1970 *High Velocity Impact Phenomena* ed R Kinslow (London: Academic)

[18] Razorenov S V, Kanel G I, Baumung K and Bluhm H J 2002 Hugoniot elastic limit and spall strength of aluminum and copper single crystals over a wide range of strain rates and temperatures *AIP Conf. Proc.* **620** 503–6

[19] Vignjevic R, Bourne N K, Millet J C and De Vuyst T 2002 Effects of orientation on the strength of the aluminum alloy 7010-T6 during shock loading: experiment and simulation *J. Appl. Phys.* **92** 4342–8

[20] Boustie M and Cottet F 1991 Experimental and numerical study of laser induced spallation into aluminum and copper targets *J. Appl. Phys.* **69** 7533–8